nature nanotechnology

LETTERS

PUBLISHED ONLINE: 8 DECEMBER 2013 | DOI: 10.1038/NNANO.2013.257

A synthetic DNA motor that transports nanoparticles along carbon nanotubes

Tae-Gon Cha[1], Jing Pan[1], Haorong Chen[1], Janette Salgado[1], Xiang Li[2], Chengde Mao[2] and Jong Hyun Choi[1]*

Intracellular protein motors have evolved to perform specific tasks critical to the function of cells such as intracellular trafficking and cell division[1,2]. Kinesin and dynein motors, for example, transport cargoes in living cells by walking along microtubules powered by adenosine triphosphate hydrolysis[3,4]. These motors can make discrete 8 nm centre-of-mass steps and can travel over 1 μm by changing their conformations during the course of adenosine triphosphate binding, hydrolysis and product release[5,6]. Inspired by such biological machines, synthetic analogues have been developed including self-assembled DNA walkers that can make stepwise movements on RNA/DNA substrates[7–12] or can function as programmable assembly lines[13]. Here, we show that motors based on RNA-cleaving DNA enzymes[14] can transport nanoparticle cargoes—CdS nanocrystals in this case—along single-walled carbon nanotubes. Our motors extract chemical energy from RNA molecules decorated on the nanotubes and use that energy to fuel autonomous, processive walking through a series of conformational changes along the one-dimensional track. The walking is controllable and adapts to changes in the local environment, which allows us to remotely direct 'go' and 'stop' actions. The translocation of individual motors can be visualized in real time using the visible fluorescence of the cargo nanoparticle and the near-infared emission of the carbon-nanotube track. We observed unidirectional movements of the molecular motors over 3 μm with a translocation velocity on the order of 1 nm min^{-1} under our experimental conditions.

The design of our synthetic molecular motor is presented in Fig. 1a, with CdS nanocrystals and carbon nanotubes used in a model system for the cargo and a one-dimensional track. Single-stranded DNA enzyme is attached to the CdS nanocrystal (shown in yellow) base pairs with an RNA molecule (a 41-base-long chimeric DNA/RNA oligonucleotide with an rA and an rU, in blue), which non-covalently adsorbs on the carbon-nanotube surface. We used the 10-23 DNA enzyme (10-23 DNAzyme, the 23rd clone after the 10th round of *in vitro* selection)[14], which has two recognition arms (red: 7-base-long upper arm and 16-base-long lower arm) and one catalytic core (green: 15 nucleotides). This oligonucleotide cleaves the phosphodiester bond between the rA and rU (pink) of the RNA fuel strand in the presence of metal cations such as Mg^{2+} (ref. 14). The walking principle of the molecular motors is schematically described in Fig. 1b. Initially, two recognition arms of the DNAzyme (E) associate with an RNA molecule (S1) on the nanotube track, which is immobilized on an agarose film (i). Metal-assisted DNAzyme cleavage of S1 results in two oligonucleotide fragments (ii)[15]: a 13-base-long fragment (P1) and a 28-base-long fragment (P2). This catalytic cleavage reaction dominates over ligation, as the cleavage rate k_{cat} is three orders of magnitude greater than the ligation rate $k_{ligation}$ (ref. 15). The P1 then dissociates from E at a rate k_D and diffuses away in the microchannel (iii), where the motor-containing polymer film is embedded (Fig. 1c). The unpaired, free recognition arm of the DNAzyme searches for and binds to an adjacent RNA molecule (S2) on the nanotube track with forward and reverse rates k_H and k_{-H} (iv). The short duplex formation is followed by a strand replacement through branch migration at a rate of k_M, transitioning to a more thermodynamically stable state (v)[16]. This strand displacement of the lower recognition arm may be understood as a single step of pseudo-continuous transition rather than two separate reactions of global melting and hybridization[17]. Overall, the DNAzyme moves from one RNA strand to the next (S1 → S2), completing a so-called single turnover. Repeated operations of the DNAzyme create a processive walking along the RNA-functionalized nanotube track without any human intervention. This 'burnt-bridge' mechanism imposes unidirectional movements of the motors, which is different from diffusive ATP-fuelled protein motors that can take forward or backward steps, but making overall unidirectional trajectories[18].

A typical nanoparticle-carrying DNA motor on the nanotube track is shown in the atomic force microscope (AFM) image in Fig. 1d (Supplementary Fig. 4). The height profile indicates that the CdS nanoparticle has a diameter of ~4 nm, while the RNA-adsorbed single-walled carbon nanotube is ~1–2 nm high along the tube axis. From optical density measurements, ~40 RNA molecules are estimated to adsorb per 100-nm-long nanotube[19]. For a typical 4-nm-diameter nanocrystal, we estimate ~20 DNAzyme strands, which is in a good agreement with our previous theoretical simulation results of 15–30 strands per particle (see Supplementary Section 'Materials and methods')[20]. Importantly, we observed almost identical translocation kinetics with a motor comprising approximately two DNAzymes/particle, suggesting that only one DNAzyme is involved in motor operation despite there being multiple strands per particle (Supplementary Figs 16, 19 and 20). We used visible and near-infrared fluorescence images to visualize the nanocrystal and nanotube, respectively. The mobile DNAzyme-functionalized nanoparticle was monitored in real time against the immobilized carbon-nanotube track by overlaying the visible and near-infrared images obtained using a wide-field optical microscope equipped with a CCD (charge-coupled device) and an InGaAs camera (Fig. 1e, Supplementary Fig. 7). This dual visible/near-infrared spectroscopy can be used for single-molecule studies[21–23] over long periods of time using photostable nanomaterial fluorophores[24–27]. Spectral measurement of carbon-nanotube emission verified the single nanotube track (Supplementary Fig. 12). Intermittent blinking of nanocrystal emission confirmed a single-particle identity on the nanotube track (Supplementary Fig. 11). We recorded the motor image periodically (for example,

[1]School of Mechanical Engineering, Bindley Bioscience Center, Birck Nanotechnology Center, Purdue University, West Lafayette, Indiana 47907, USA, [2]Department of Chemistry, Purdue University, West Lafayette, Indiana 47907, USA. *e-mail: jchoi@purdue.edu

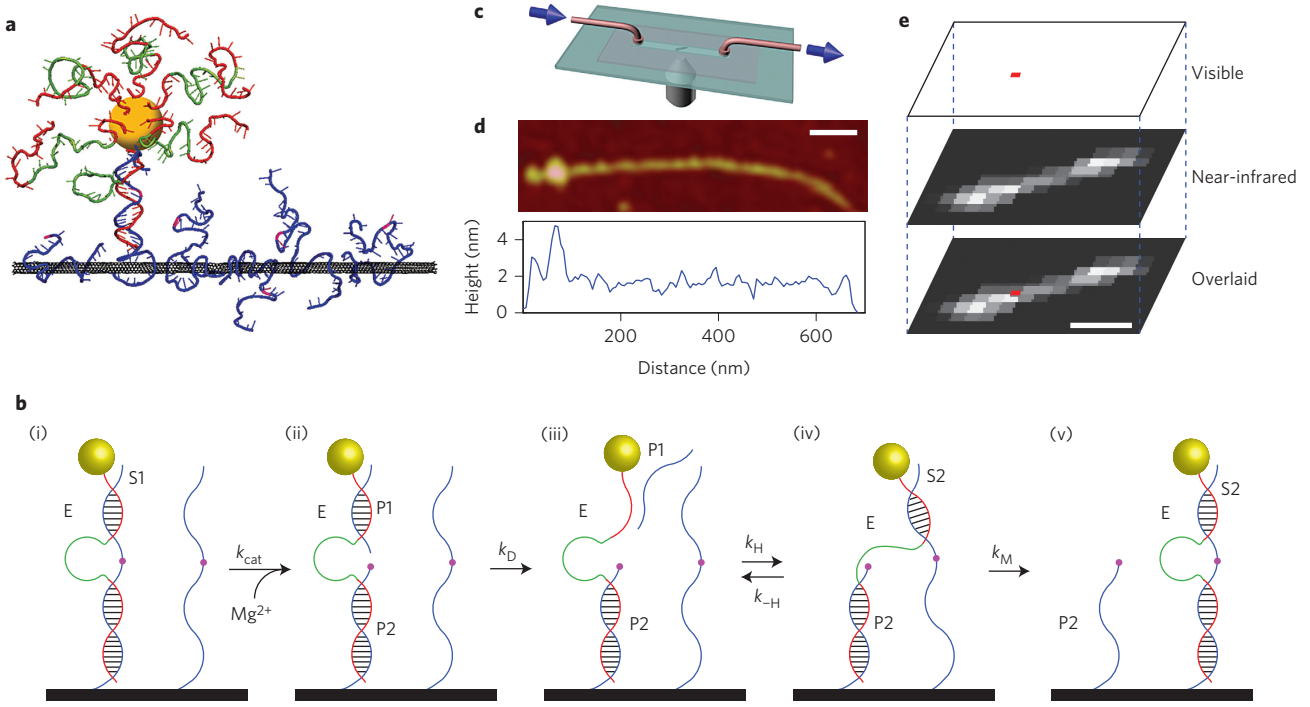

Figure 1 | The DNAzyme-based molecular motor that moves along a carbon-nanotube track. a, Molecular model of a nanoparticle-functionalized, 10-23 DNAzyme-based motor on an RNA-decorated nanotube track. The DNAzyme motor consists of a catalytic core (green) and two recognition arms (red). CdS nanocrystals (yellow) and carbon nanotubes (black) are used as a model system for the cargo and a one-dimensional track. The DNAzyme motor converts the chemical energy of RNA into mechanical motion through a series of DNA conformation changes, walking along the nanotube track processively and autonomously, similar to intracellular protein motors. **b**, Walking principle of the DNAzyme-based motor. After associating with an RNA (S1), the DNAzyme (E) cleaves S1 (pink) in the presence of Mg^{2+}, producing short (P1) and long (P2) fragments. P1 then dissociates from E, and the unbound recognition arm of E associates with an adjacent RNA (S2) on the track. The rest of the E migrates from S1 to S2, completing a single turnover. By repeating the process, the molecular motor moves along the nanotube track without human intervention. **c**, Schematic of the flow-through chamber, in which the nanotube is immobilized on an agarose film. Buffer change is performed only between the experiments to avoid any flow-induced drag effects. **d**, AFM image of the molecular motor and the corresponding height profile along the nanotube. The CdS nanoparticle has a diameter of ~4 nm, and the RNA-adsorbed carbon-nanotube track is ~1–2 nm high. Scale bar, 100 nm. **e**, Optical characterization method. The motor movement is monitored with a home-built, inverted fluorescence microscope with a visible CCD and a near-infrared camera. The pseudo-coloured fluorescence image of the CdS nanocrystal (top) is overlaid with the near-infrared nanotube image (middle). The location of the mobile nanoparticle relative to the immobile nanotube (bottom) is periodically determined as a function of time during the experiments. Scale bar, 2 μm.

every few hours) to allow it to travel sufficiently long distances, thereby overcoming the optical resolution limit of ~250 nm.

Optical detection of the DNA-based molecular motor translocation along a nanotube is shown in Fig. 2a. The position of the nanoparticle (red spots indicated by yellow arrows) moves continuously from the centre of the nanotube to the left edge in tris-acetate-ethylenediaminetetraacetic acid (TAE) buffer with 100 mM Mg^{2+} at 22 °C and pH 8.0. The trajectory of the motor, travelling ~3 μm in 30 h, is also indicated (yellow arrow in rightmost panel). Twenty hours after the experiment started, we observed minute changes in motor translocation, indicating that the motor had reached the end of the nanotube track. The autonomous operation of the cargo-carrying motor requires RNA to be bound to the track to serve as fuel. To confirm the motor walking, we performed three sets of control experiments that prohibited the catalytic cleavage of RNA by the DNA motor. We first mutated the DNAzyme sequence so that the DNA strands did not have catalytic cores, while the RNA strands were held constant. All other conditions were identical during the measurements. In the second experiment, the cleavage point of the RNA molecules was omitted, while the DNA enzyme sequence was kept intact. Finally, we ran the translocation experiment with the motor made of intact DNAzyme and RNA sequences under the same buffer conditions except for the removal of metal cations (that is, 0 mM Mg^{2+}). In all three cases, we did not observe significant movements over time (Supplementary Figs 21–24). The motor locations were recorded every 4 h, and a travel distance of ~100 nm was observed each time, which is within the uncertainty of our measurements. The mobility of our motor was also verified by incorporating a mobile, intact DNAzyme (red spots indicated by yellow arrows, Fig. 2b) and an immobile, mutated DNAzyme without the catalytic core (blue spots indicated by white arrows) on a nanotube track. The red dot travelled continuously towards the blue dot in the TAE buffer with 100 mM Mg^{2+}, whereas the blue dot remained stationary during the 12 h observation.

The programmed operation of the cargo-carrying motor on the one-dimensional track can be controlled remotely. Given that the motor mechanics require metal cations for RNA hydrolysis, we regulated the metal cation concentration in the flow-through chamber to direct go and stop actions. During the first 8 h, TAE buffer with 100 mM Mg^{2+} (the go signal) was supplied to promote the motor operation, resulting in motor translocation over 1.2 μm (Fig. 2c). In the following 8 h, fresh buffer with 0 mM Mg^{2+} (the stop signal) was provided while all other conditions were held constant. Buffer change was performed only between experiments, and between each measurement no flow was introduced to avoid any flow-induced drag effects. As anticipated, no significant movement was observed during this period. The go and stop signals were then sequentially repeated to ensure the temporal and spatial fidelity of the movement.

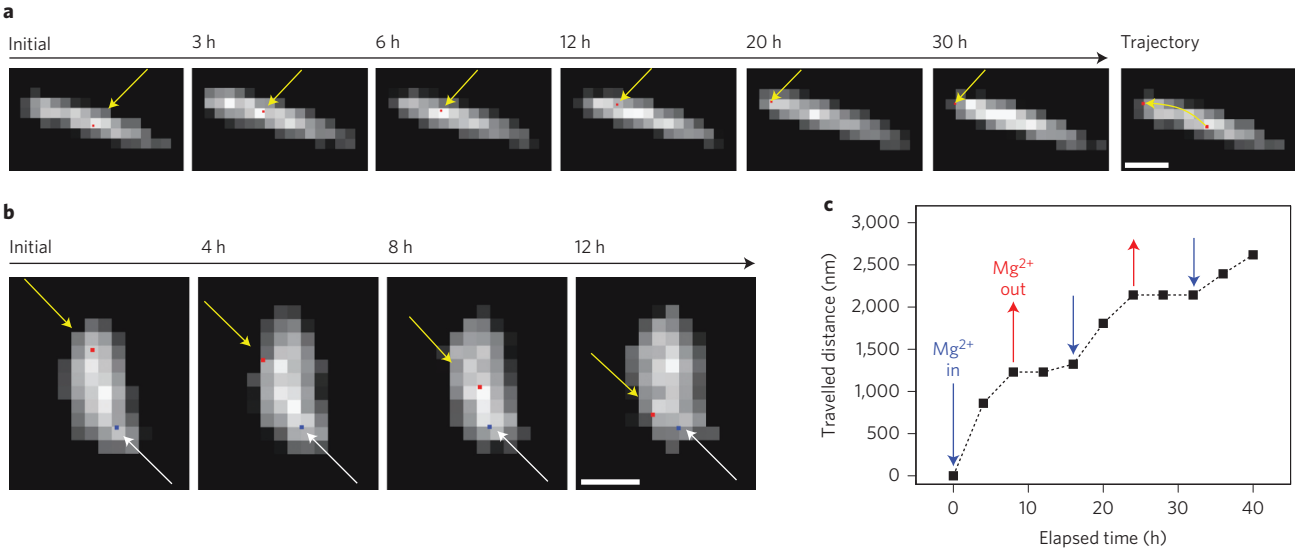

Figure 2 | Molecular motor movement in TAE buffer at 22 °C and pH 8.0. a, Motor images recorded over 30 h in the presence of 100 mM Mg^{2+}. Yellow arrows indicate the positions of the nanoparticle (red squares). The trajectory of the molecular motor is also shown (rightmost image). Scale bar, 2 μm. **b**, A mobile DNAzyme (red squares indicated by yellow arrows) and an immobile, mutated DNAzyme without the catalytic core (blue squares indicated by white arrows) are observed on a carbon-nanotube track with 100 mM Mg^{2+}. The stationary blue dot is the pseudo-coloured image of the CdS nanocrystal with the mutated DNAzyme sequence. Scale bar, 2 μm. **c**, Motor translocation as a function of Mg^{2+}. Initially, the motor movement was monitored with 100 mM Mg^{2+} every 4 h. After 8 h, metal cations were removed from the microchannel by flowing excess buffer (0 mM Mg^{2+}), and their positions were recorded over the next 8 h. In the absence of divalent cations, the motor did not show any significant movement. For 16–24 h, TAE buffer with 100 mM Mg^{2+} was reintroduced to facilitate the motor movement. Then, Mg^{2+} was removed from the chamber until 32 h, when the ions were reintroduced. The motor walking is evident in the presence of Mg ions, whereas no significant movement is observed in their absence.

To understand how environmental factors affect motor operation, we measured the distance travelled by the molecular motor while varying the conditions, including concentration, type of metal cation, buffer temperature and pH. In Fig. 3a, the molecular motor movement is examined as a function of Mg ion concentration in TAE buffer at 22 °C and pH 8.0. Given the processive walking, the translocation velocity was determined by linear fitting. The values of translocation velocities were ~120, 160 and 220 nm h^{-1} at 10, 50 and 100 mM Mg^{2+}, respectively. The translocation velocity increases with ionic strength, but levels off above an observed threshold indicated by nearly identical travel distances over the same time period at 200 mM Mg^{2+} (Supplementary Fig. 30). We also explored other metal cations such as Ca^{2+} and K^{+} (Supplementary Figs 31–38). The translocation velocities in the presence of Ca^{2+} at 10, 50 and 100 mM concentrations were estimated to be ~110, 140 and 150 nm h^{-1}, suggesting that Ca ions are somewhat less efficient than Mg ions. However, the motor velocity was notably slower with monovalent K ions than divalent cations under identical experimental conditions (~45, 60 and 70 nm h^{-1} at 10, 50 and 100 mM K^{+} concentrations).

The thermal environment is expected to considerably influence the motor activities, because the cleavage reactions of the DNAzyme strand with RNA as well as base-pairing and dissociation processes are temperature-dependent[28]. The translocation velocity was examined at various temperatures (Fig. 3b); as expected, the molecular motor displayed increased translocation velocities with higher buffer temperature. A gradual increase in translocation velocity was also observed while varying the pH from 6.5 to 9.0 (Fig. 3c). Because the DNAzyme catalytically attacks and deprotonates the 2′-hydroxyl group of RNA strands near the cleavage point with the help of metal cations, this process should be facilitated at high pH. The results also suggest that the increase in cleavage rate is steeper at lower pH ranges than at higher pH ranges. This pH-dependent catalytic RNA cleavage behaviour is consistent with free DNA enzyme studies in ensemble measurements[15].

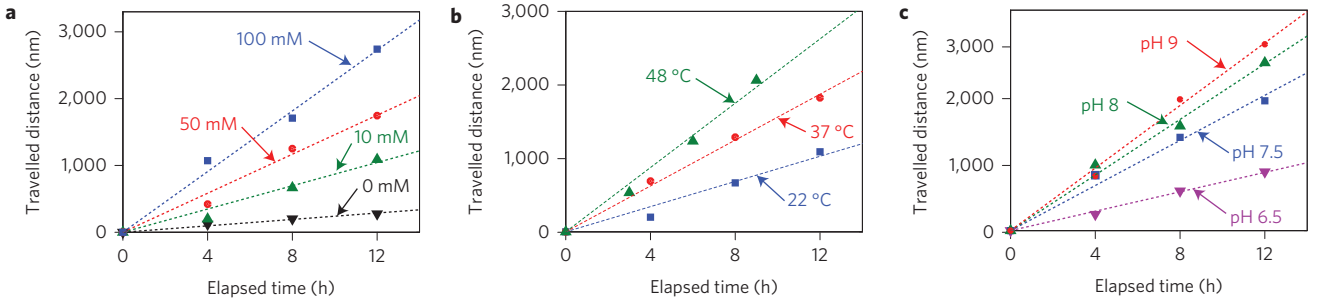

Figure 3 | Local environmental effects on the mobility of the molecular motors in TAE buffer. a, The effect of Mg^{2+} concentrations on the speed of the molecular motor at 22 °C and pH 8.0. The linearly fitted dotted lines indicate the translocation velocities of the molecular motor under given conditions. **b**, The temperature dependence of motor translocation at 10 mM Mg^{2+} and pH 8.0. **c**, Buffer pH dependence of motor movement at 100 mM Mg^{2+} and 22 °C. A gradual increase in translocation velocity was observed with increasing pH from 6.5 to 9.0.

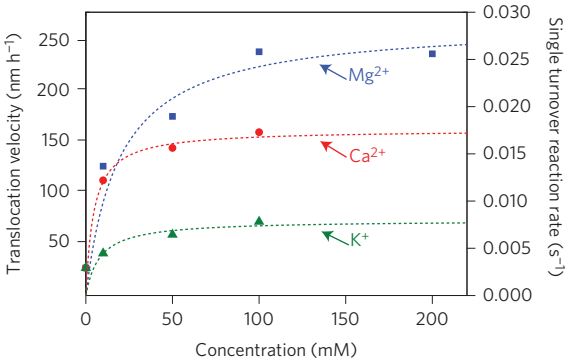

Figure 4 | Experimental and theoretical translocation kinetics of the molecular motor. Translocation velocities of the molecular motor were experimentally determined for various metal cations and their concentrations at 22 °C and pH 8.0. A simple kinetic model of a single motor, developed within the framework of single-molecule kinetics, reveals single turnover rates (shown as dotted curves). The experimental results of motor translocation were converted into the single turnover reaction rate considering the estimated distance between two adjacent RNA substrates. The simulation results suggest that the cleavage reaction rates (k_{cat}) of the molecular motor are ~0.096 s^{-1} with Mg^{2+}, ~0.144 s^{-1} with Ca^{2+} and ~0.067 s^{-1} with K^+. The simulations also indicate branch migration rates (k_M) of ~0.211, 0.039 and 0.011 s^{-1} with Mg^{2+}, Ca^{2+} and K^+, respectively. Under the saturation of cationic conditions, of the three metal ions examined, the molecular motor exhibits the greatest overall reaction rate with Mg^{2+}; ~40 s is required to move from one RNA fuel strand to the next.

A simple kinetic model was developed within the framework of single-molecule kinetics to quantitatively understand the single turnover reaction from states (i) to (v) in Fig. 1b. A set of concentration-based rate equations describing the series of DNA conformation change reactions were converted into probability-based rate equations[29], which were numerically solved to predict the rates for each reaction step as well as the single turnover event (see Supplementary Section 'Kinetic model'). Figure 4 shows the experimental and theoretical translocation kinetics of the motor as functions of cationic type and concentration. Two divalent cations (Mg^{2+} and Ca^{2+}) and one monovalent ion (K^+) were examined for their ability to facilitate the cleavage of the RNA fuels, thereby propelling the motor along the nanotube track. The simulated kinetic results (dotted curves in Fig. 4) reasonably predict the measured velocities (symbols; also see Supplementary Figs 26–38). The simulations suggest that the cleavage reaction rates with Mg^{2+} and Ca^{2+} are ~0.096 and 0.144 s^{-1} for 100 mM Mg^{2+} at pH 8.0, which are comparable to those from ensemble measurements in the free-solution DNAzyme studies under similar conditions[15]. The catalytic cleavage reaction rate was found to be lowest at ~0.067 s^{-1} in the presence of the monovalent K ions, with all other conditions constant. The simulations also indicate that k_M is faster with Mg^{2+} at ~0.211 s^{-1} than with Ca^{2+} at ~0.039 s^{-1}, which is not unexpected given that the branch migration is strongly dependent on the type of metal ion[30]. Overall, the reaction rate for the single turnover event under the saturation of cationic conditions is greater with Mg than Ca as measured experimentally. Approximately 40 s are required for the single turnover reaction under our experimental conditions with saturation of Mg^{2+}; that is, the time for the DNA motor to move from one RNA fuel strand to the next. A closer examination of this simulation result reveals that the reaction steps from (i) to (v) take ~10, 25, 0.2 and 4.8 s, respectively, suggesting that the kinetics strongly depends on the catalytic core type (k_{cat}) and recognition arm lengths (k_D, k_H and k_M). We anticipated and observed that the catalytic core with a greater cleavage reaction rate leads to a higher translocation velocity with all other conditions identical (Supplementary Fig. 44). For a given catalytic core, we find that the motors with a short upper arm and a long lower arm demonstrate greater motility than the ones with a long upper arm and a short lower arm (for example, 7-16 versus 16-7 nucleotide recognition arms). These results suggest that the dissociation of the upper recognition arm is the rate-limiting step when compared to the cleavage reaction and branch migration in our motor translocation experiments (Supplementary Fig. 45).

Finally, an all-synthetic DNA motor system is demonstrated. This system is distinct in that a DNA motor walks several micrometres along a non-DNA track, carrying an inorganic cargo. The maximum velocity measured in this study was ~0.1 nm s^{-1}, which is similar to the velocities of other DNA motors that walk on DNA origami platforms[11,12]. The dual visible/near-infrared optical spectroscopy enables real-time, *in situ* observation of individual motor movements, allowing one to explore the effects of critical parameters on single motor kinetics. Compared to AFM imaging, this optical platform is better suited to long-term, non-invasive measurements and should facilitate future studies of molecular machines. In particular, the catalytic core type and the length of recognition arms may be further explored to improve the motor mechanics and motility. Such design criteria can be rationalized by the kinetic model, which is used in evaluating enzymatic and other motor activities at the single-molecule level.

Methods

Materials synthesis. The 10-23 DNA enzyme (DNAzyme: 5′-AGT GCT GAT TCG GAC AGG CTA GCT ACA ACG AGA GTG AC-3′) and RNA (5′-TTT TTG TCA CTC rArUG TCC GAA TCA GCA CTT TTT TGT CAC TC-3′) strands were custom-synthesized by Integrated DNA Technologies. CdS nanocrystals were synthesized using $CdCl_2$, Na_2S and DNAzyme strands, and as-synthesized nanocrystals were washed to remove unbound excess strands and ions[21]. The RNA-functionalized carbon nanotubes were prepared via a two-stage dialysis with sodium cholate dispersed single-walled carbon nanotubes. The RNA-functionalized carbon nanotubes were immobilized on a 2 wt% agarose film, which was placed in a flow-through chamber before experiments. TAE buffer was used throughout the experiments.

Optical characterization. A home-built fluorescence microscope system was used to visualize the translocation of the molecular motors. The near-infrared photoluminescence images of RNA-coated carbon nanotubes were recorded using an OMA-V two-dimensional liquid-nitrogen-cooled InGaAs camera (Princeton Instruments, 320 × 256 photodiodes) with 658 nm diode laser excitation. The visible photoluminescence images of the DNAzyme-functionalized CdS nanocrystals were collected by a CCD camera (AxioCam MRm, 1,388 × 1,040 pixels) with 405 nm laser diode excitation.

Received 15 July 2013; accepted 30 October 2013; published online 8 December 2013

References

1. Vale, R. D. The molecular motor toolbox for intracellular transport. *Cell* **112,** 467–480 (2003).
2. Finer, J. T., Simmons, R. M. & Spudich, J. A. Single myosin molecule mechanics—piconewton forces and nanometre steps. *Nature* **368,** 113–119 (1994).
3. Hirokawa, N. Kinesin and dynein superfamily proteins and the mechanism of organelle transport. *Science* **279,** 519–526 (1998).
4. Howard, J., Hudspeth, A. J. & Vale, R. D. Movement of microtubules by single kinesin molecules. *Nature* **342,** 154–158 (1989).
5. Block, S. M., Goldstein, L. S. B. & Schnapp, B. J. Bead movement by single kinesin molecules studied with optical tweezers. *Nature* **348,** 348–352 (1990).
6. Yildiz, A., Tomishige, M., Vale, R. D. & Selvin, P. R. Kinesin walks hand-over-hand. *Science* **303,** 676–678 (2004).
7. Bath, J., Green, S. J. & Turberfield, A. J. A Free-running DNA motor powered by a nicking enzyme. *Angew. Chem. Int. Ed.* **44,** 4358–4361 (2005).
8. Yin, P., Choi, H. M. T., Calvert, C. R. & Pierce, N. A. Programming biomolecular self-assembly pathways. *Nature* **451,** 318–322 (2008).
9. Omabegho, T., Sha, R. & Seeman, N. C. A bipedal DNA Brownian motor with coordinated legs. *Science* **324,** 67–71 (2009).
10. He, Y. & Liu, D. R. Autonomous multistep organic synthesis in a single isothermal solution mediated by a DNA walker. *Nature Nanotech.* **5,** 778–782 (2010).
11. Lund, K. *et al.* Molecular robots guided by prescriptive landscapes. *Nature* **465,** 206–210 (2010).

12. Wickham, S. F. J. *et al.* Direct observation of stepwise movement of a synthetic molecular transporter. *Nature Nanotech.* **6,** 166–169 (2011).
13. Gu, H. Z., Chao, J., Xiao, S. J. & Seeman, N. C. A proximity-based programmable DNA nanoscale assembly line. *Nature* **465,** 202–205 (2010).
14. Santoro, S. W. & Joyce, G. F. A general purpose RNA-cleaving DNA enzyme. *Proc. Natl Acad. Sci. USA* **94,** 4262–4266 (1997).
15. Santoro, S. W. & Joyce, G. F. Mechanism and utility of an RNA-cleaving DNA enzyme. *Biochemistry* **37,** 13330–13342 (1998).
16. Tian, Y., He, Y., Chen, Y., Yin, P. & Mao, C. D. Molecular devices—a DNAzyme that walks processively and autonomously along a one-dimensional track. *Angew. Chem. Int. Ed.* **44,** 4355–4358 (2005).
17. Zhang, D. Y. & Seelig, G. Dynamic DNA nanotechnology using strand-displacement reactions. *Nature Chem.* **3,** 103–113 (2011).
18. Block, S. M. Kinesin motor mechanics: binding, stepping, tracking, gating, and limping. *Biophys. J.* **92,** 2986–2995 (2007).
19. Jeng, E. S., Moll, A. E., Roy, A. C., Gastala, J. B. & Strano, M. S. Detection of DNA hybridization using the near-infrared band-gap fluorescence of single-walled carbon nanotubes. *Nano Lett.* **6,** 371–375 (2006).
20. Cha, T.-G. *et al.* Understanding oligonucleotide-templated nanocrystals: growth mechanisms and surface properties. *ACS Nano* **6,** 8136–8143 (2012).
21. Tsyboulski, D. A., Bachilo, S. M. & Weisman, R. B. Versatile visualization of individual single-walled carbon nanotubes with near-infrared fluorescence microscopy. *Nano Lett.* **5,** 975–979 (2005).
22. Cognet, L. *et al.* Stepwise qeunching of exciton fluorescence in carbon nanotubes by single-molecule reactions. *Science* **316,** 1465–1468 (2007).
23. Dahan, M. *et al.* Diffusion dynamics of glycine receptors revealed by single-quantum dot tracking. *Science* **302,** 442–445 (2003).
24. Carlson, L. J. & Krauss, T. D. Photophysics of individual single-walled carbon nanotubes. *Acc. Chem. Res.* **41,** 235–243 (2008).
25. Alivisatos, A. P. The use of nanocrystals in biological detection. *Nature Biotechnol.* **22,** 47–52 (2004).
26. Choi, J. H. & Strano, M. S. Solvatochromism in single-walled carbon nanotubes. *Appl. Phys. Lett.* **90,** 223114 (2007).
27. Bachilo, S. M. *et al.* Structure-assigned optical spectra of single walled carbon nanotubes. *Science* **298,** 2361–2366 (2002).
28. Schubert, S. *et al.* RNA cleaving '10–23' DNAzymes with enhanced stability and activity. *Nucleic Acids Res.* **31,** 5982–5992 (2003).
29. Kou, S. C., Cherayil, B. J., Min, W., English, B. P. & Xie, X. S. Single-molecule Michaelis–Menten equations. *J. Phys. Chem. B* **109,** 19068–19081 (2005).
30. Panyutin, I. G. & Hsieh, P. The kinetics of spontaneous DNA branch migration. *Proc. Natl Acad. Sci. USA* **91,** 2021–2025 (1994).

Acknowledgements

The authors thank H.N. Robinson and M.C. Akatay for help with synthesis and TEM characterization of CdS nanocrystals. This work was supported by the US Office of Naval Research (awards N00014-11-1-0220 and N00014-12-1-0829). J.H.C. acknowledges a National Science Foundation Career award.

Author contributions

J.H.C. and C.M. conceived the idea. J.H.C. and T.G.C. designed the research. T.G.C. synthesized materials and performed the motor translocation experiments with assistance from J.P. and J.S. H.C. and J.P. collected AFM images. C.M. and X.L designed the oligonucleotide motifs. T.G.C. and J.H.C. developed the kinetic model and analysed the data. J.H.C. and T.G.C. co-wrote the paper with input from all authors.

Additional information

Supplementary information is available in the online version of the paper. Reprints and permissions information is available online at www.nature.com/reprints. Correspondence and requests for materials should be addressed to J.H.C.

Competing financial interests

The authors declare no competing financial interests.